Khulna University Studies Special Issue ICSTEM4IR: 307-320, 2022

ORIGINAL ARTICLE

SCIENCE & ENGINEERING

Copyright©Khulna University

RADIATION AND HALL CURRENT IMPRESSIONS ON NEWTONIAN AND BINGHAM FLUIDS FLOW PAST A STRETCHING SURFACE

Md. Yousuf Ali, Sk. Reza-E-Rabbi*, Sarder Firoz Ahmmed*

Mathematics Discipline, Khulna University, Khulna- 9208

KUS: ICSTEM4IR-22/0014

Manuscript submitted: August 11, 2022 Accepted: September 26, 2022

Abstract

The continuous two-dimensional MHD nanofluid flow across a nonlinear stretching sheet has been investigated in this work. In this paper, the study was done in the presence of both Hall current and radiation. The nonlinear partial differential equations were first regulated using boundary layer approximation, and then the governing equations were converted into an ordinary system of differential equations using appropriate similarity solutions. The numerical simulations were carried out using the Nachtsheim-Swigert shooting iteration approach and a six-order Runge-Kutta integration scheme where a programming language called FORTRAN was used as assistance. The outcomes of the problem related equations have been narrated briefly and displayed by various graph. The dominance of the stretching parameter and combined effects of Hall current together with thermal radiation on velocity profiles, temperature profiles, and concentration profiles, as well as important physical phenomena like skin friction, Nusselt number and Sherwood number, were examined with the help of various graphs. The implications of material and magnetic factors on primary velocity, Prandtl number on temperature profiles, and Lewis number on concentration profiles have been visually depicted. The dominance of Hall current and radiation at the same time, as well as the impression of stretching parameter, have been determined to be more effective on Bingham fluid. It has application in drug delivery. It can be used to administer drugs. Because fluidity takes a particular level of shear stress to produce, it may be focused to medication delivery in certain muscles or organs by regulating injection pressure and other drug delivery devices.

Keywords: Hall Current, Thermal radiation, Stretching Sheet, Bingham fluid, RK-based shooting method.

Introduction

Recently, many of the researcher keeping in mind that the applications of the boundary layer flow of the MHD nanofluid over a nonlinear stretching sheet have been investigated. Many of the platform such as pumps, heat exchanger, thermal protection, controlling fusion, vehicle propulsion, etc. are schematic and manufactured on the principles of MHD. According to above applications the fluid mechanical features of the penult product mainly figure on two things such as the rate of stretching and use of cooling liquid. Iva *et al.* (2018) researched

*Corresponding author: <rabbi06@math.ku.ac.bd; sfahmmed@math.ku.ac.bd>
DOI: https://doi.org/10.53808/KUS.2022.ICSTEM4IR.0014-se

about the free convection flow including the mass and heat transfer of MHD fluid in presence of Hall current above a perpendicular porous plate and the system was rotating. Hall current, heat source and suction effect were also included in their experiment. The dimensional governing equations of this experiment were composed by using an explicit finite difference method after nondimensionalized. The impacts on the velocity, temperature and concentration profiles are plotted for various parameters. The different profiles were also separately discussed with the help of different graphical representation.

Mahmood *et al.* (2017) investigated the Sisko fluid containing nanoparticles, which past a stretching (non-linear) sheet. The combined effects of magneto hydrodynamics and radiation on the sisko nanofluid had been examined in this paper. The effects of Brownian motion and thermophoresis were also considered in their paper. The governing equations were solved with the help of BVP4c method in MATLAB after the transformation of the partial differential equation to ordinary differential equation. They also discussed the velocity profiles, concentration profiles and temperature profiles for various parameters and the results are analyzed through several graphs. The heat transference study on mixed convective flow had been performed by Ramzan *et al.* (2021), where the magnetohydrodynamics hybrid nanofluid flow past a stretching sheet in presence of slip conditions. The influence of different parameters on velocity and thermal profiles is narrated as well as the skin friction coefficient and Nusselt number with the help of several graphs. The influence of thermophoretic particle deposition above the 3D flow was studied by Shankaralingappa *et al.* (2021) and the flow was considered over a stretching sheet. The nanofluid was considered as the mixed of sodium alginate-based Casson fluid and the flow was considered over a stretching sheet. The Runge Kutta Fehlberg 4^{th} 5^{th} order scheme with shooting technique has been employed to obtain the numerical outcomes. The effects of different parameters on the fluid flow had been deliberated and illustrated with the help of various graph of the numerical outcomes. Sahoo *et al.* (2021) investigated on mixed convective hydromagnetic Casson nanofluid flow in presence of thermal radiation with Hall current. The main purpose of their work was to analyze the entropy generation and heat transfer of mixed convective flow. They discussed briefly the influence of the various non-dimensional flow parameters on the velocity profiles, temperature profiles and concentration profiles as well as entropy generation and Bejan number with the help of different graphical illustration. Bilal *et al.* (2021) researched on swirling flow of Newtonian liquid where the liquid was magnetically affected and the fluid flow induced by porous disk. After transformation of the partial differential equations into ordinary differential equations, implicitly finite differenced scheme which is also known as the Keller Box technique was employed to get the numerical solutions. Actually, the influence of flow which was controlled by different parameters were exposed with the help of different graph and tabular representations. Reddy *et al.* (2021) studied on MHD Casson fluid flow with the presence of radiation and heat source or sink and the flow considered over a stretching sheet due to slip conditions. The motive of that work was narrated the influence of non-dimensional parameters on the velocity, temperature and concentration distributions with the help of distinct graphical illustration. The study on radiative magnetohydrodynamics Casson nanofluid flow past a nonlinear stretching surface was investigated by Thirupathi *et al.* (2021) with heat and mass transfer. A nonlinear stretching surface was approached as the medium of fluid flow with velocity slip and viscous dissipation, heat source and chemical reaction had also been considered. To obtain the numerical solution, shooting technique was engaged with the help of Adams-Moulton method of order four. The impacts of various physical parameters were deliberated by graphically and also discussed as well as the skin friction coefficient, Nusselt number and Sherwood number.

An unsteady MHD nanofluid flow was investigated by Muntazir *et al.* (2021), where a permeable linearly stretching sheet had been used with the influence of thermal radiation and viscous dissipation. Their investigation was thought for different kinds of nano-particles such as Al2O3, Cu, Ag and TiO2. The semi-analytical technique namely Differential Transformation Method (DTM) was engaged for the numerical simulations and the numerical solutions were illustrated and discussed with the help of several graphical representation and narrated the behavior of fluid flow. Ragupathi *et al.* (2021), studied computationally on three dimensional convective Casson nanofluid flow in presence of Arrhenius activation energy and

exponential heat source with the convective flow past a stretching sheet. The non-Newtonian fluid was considered in their work and the IPS technique had been applied to obtain the numerical solutions from the ordinary differential equations. They analyzed the behavior of several capable physical parameters and displayed some graphical representation. The investigation of thermal and chemically reactive features of Casson nanofluid flow were performed by Khan *et al.* (2021), where an exponentially stretching surface had been considered in appearance of thermophoresis and Brownian motion. For numerical simulations of the obtaining ordinary differential equation from partial differential equations, bvp4c technique had been used by them with the help of MATLAB coding. The physical quantities had been discussed with graphical representation and tabulating data. Stefan blowing impression on unsteady MHD flow had been studied by Haider *et al.* (2021) with electric field, thermal radiation and activation energy. The magnetohydrodynamics nanofluid flow over a stretching sheet were investigated by them. They solved the obtaining nonlinear ordinary differential equations by applying the Runge-Kutta 4th order using the shooting technique in MATLAB software and the numerical outcomes were discussed appropriately with the help of tabular and graphical representation.

Keeping in mind the extensive applications of MHD and inspired by the above discussions, the goal of this work is to examine the impression of stretching rate with Hall current and radiation on Bingham and Newtonian fluids. The present project has been categorized and key motives of this work are as follows:

- To formulate the problem related mathematical equations namely momentum equation, energy equation and concentration equation with the associate boundary conditions.
- To transform the problem related partial differential equations into the ordinary differential equations by using appropriate similarity transformations.
- To obtain the numerical solutions, the Nachtsheim-Swigert shooting iteration method with six order R-K integration scheme have been applied with the help of FORTRAN 6.6a programing language.
- To investigate the impression of fluid related parameters on velocity, temperature and concentration as well as some vital physical parameters namely skin friction, Nusselt number Sherwood number.
- Mainly, to analyze the effect of the stretching rate on velocity, temperature and concentration profiles with skin friction, Nusselt number and Sherwood number at the same time.

Materials and Methods

Mathematical formulation

Two-dimensional radiative steady flow in presence of Hall current on MHD nanofluid in the section $y > 0$. The fluid flow past a non-linear stretching sheet along the power-law velocity $U_0 = ax^n$ and n be the stretching rate with $n \geq 0$. The sheet is oriented with the x-axis and the y-axis is orthogonal to the sheet. Some fluid which is taken as hot with temperature T_w^* is elevated to warm or cold the surface of the sheet due to the Hall current and radiation whose have been employed to the MHD nanofluid in the approach of collateral to the x-axis with the assumption of magnetic field. The Concentration of the nanoparticle is possessed the base of the stretching sheet is C_w^*, while the inclusive concentration and temperature are C_∞^* and T_∞^* respectively. Now, by applying the boundary layer approximation and under the above consideration the physical representation of the problem is displayed by Figure 1 and the system of governing equations for continuity, momentum, energy and concentration of the MHD nanofluid flow are given by the equations (1) to (5) respectively, [Iva *et al.* (2018), Mahmood *et al.* (2017)]

$$\frac{\partial u}{\partial x} + \frac{\partial v}{\partial y} = 0 \tag{1}$$

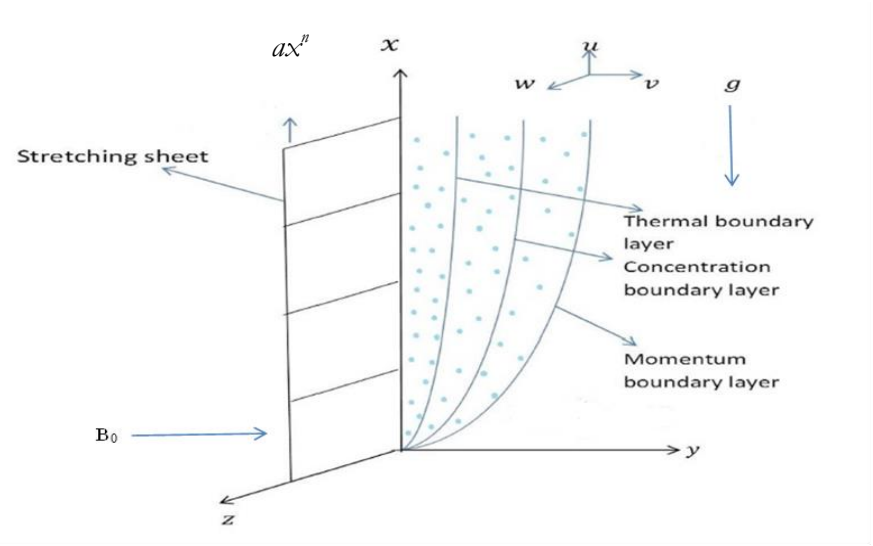

Figure 1. Physical Model of the problems.

$$u\frac{\partial u}{\partial x}+v\frac{\partial u}{\partial y}=\upsilon\frac{\partial^2 u}{\partial y^2}+g\beta^*\left(C^*-C_\infty^*\right)+g\beta\left(T^*-T_\infty^*\right)-\frac{\sigma B_0^2}{\rho\left(1+m^2\right)}\left(u+mw\right) \tag{2}$$

$$u\frac{\partial w}{\partial x}+v\frac{\partial w}{\partial y}=\upsilon\frac{\partial^2 w}{\partial y^2}+\frac{\sigma B_0^2}{\rho\left(1+m^2\right)}\left(mu-w\right) \tag{3}$$

$$u\frac{\partial T^*}{\partial x}+v\frac{\partial T^*}{\partial y}=\alpha\frac{\partial^2 T^*}{\partial y^2}+\tau\left\{D_B\left(\frac{\partial C^*}{\partial y}\frac{\partial T^*}{\partial y}\right)+\frac{D_T}{T_\infty^*}\left(\frac{\partial T^*}{\partial y}\right)^2\right\}-\frac{1}{\rho c_p}\frac{\partial q_r}{\partial y} \tag{4}$$

$$u\frac{\partial C^*}{\partial x}+v\frac{\partial C^*}{\partial y}=D_B\frac{\partial^2 C^*}{\partial y^2}+\frac{D_T}{T_\infty^*}\frac{\partial^2 T^*}{\partial y^2} \tag{5}$$

The boundary conditions for the above governing equations are taken in Equation (6),

$$\left.\begin{aligned}&u(x,y)=ax^n=U_0,\ v(x,y)=0,\ w(x,y)=0,\ T^*=T_w^*,\ C^*=C_w^*\ \text{at}\ y=0\\&u=v=w=0,\ T^*=T_\infty^*,\ C^*=C_\infty^*\ \text{as}\ y\to\infty\end{aligned}\right\} \tag{6}$$

In the above Equations (1) to (5), u and v denote the primary velocity ingredient toward the x-axis and y-axis respectively and w be secondary velocity which is obtained by applying the Hall current. The fluid density and the specific heat at constant pressure are indicated by ϱ and c_p. The acceleration due to gravity, kinematic viscosity and magnetic induction are indicated by g, ν and B_0, the thermal and concentration expansion coefficient are narrated by β and β^* respectively, a is the thermal diffusivity, m be the Hall current parameter, σ be the electrical conductivity, D_B and D_T are the Brownian and thermophoresis diffusion coefficient, $\tau\ (=(\rho c)_p/(\rho c)_f)$ indicates the ratio of effective heat capacity of nanoparticle material.

In the radiative term we have been taken by the equation as follows,

$$q_r=\frac{-4\sigma^*}{3k^*}\frac{\partial T^{*4}}{\partial y} \tag{7}$$

where k^* and σ^* indicate absorption parameter and Stefan Boltzmann constant. The difference of temperature into the flow field is possessed such that T^{*4} can be elongated in designation of Taylor series. The higher order quantities of the series can be neglected and we have been taken in Equation (8),

$$T^{*4} \cong 4T_\infty^{*3}T^* - 3T_\infty^{*3} \tag{8}$$

Let, the similarity solutions for the above equations are given in Equation (9),

$$\begin{aligned} &u = U_0 f'(\eta);\ w = U_0 g'(\eta);\ \eta = \frac{y}{x}\mathrm{Re}_b^{\frac{1}{p+1}};\ \theta(\eta) = \frac{T^* - T_\infty^*}{T_w^* - T_\infty^*};\ \phi(\eta) = \frac{C^* - C_\infty^*}{C_w^* - C_\infty^*} \\ &v = -\mathrm{Re}_b^{-\frac{1}{p+1}} \frac{U_0}{p+1}\Big[\{n(2p-1)+1\} f(\eta) + \{n(2-p)-1\}\eta f'(\eta)\Big] \end{aligned} \tag{9}$$

By using above similarity solutions (9), we get the Equations (10-13),

$$\begin{aligned} &Af'''(\eta) + \frac{n(2p-1)+1}{p+1} f(\eta) f''(\eta) - n\{f'(\eta)\}^2 + \mathrm{Re}_x \{Gr\theta(\eta) + Gm\phi(\eta)\} \\ &\qquad - \frac{M\,\mathrm{Re}_x}{1+m^2}\{f'(\eta) + mg'(\eta)\} = 0 \end{aligned} \tag{10}$$

$$Ag'''(\eta) + \frac{n(2p-1)+1}{p+1} f(\eta) g''(\eta) - nf'(\eta) g'(\eta) + \frac{M\,\mathrm{Re}_x}{1+m^2}\{mf'(\eta) - g'(\eta)\} = 0 \tag{11}$$

$$(1+N_r)\theta''(\eta) + \frac{n(2p-1)+1}{p+1}\mathrm{Pr}\, f(\eta)\theta'(\eta) + N_b\theta'(\eta)\phi'(\eta) + N_t\{\theta'(\eta)\}^2 = 0 \tag{12}$$

$$\phi''(\eta) + \frac{n(2p-1)+1}{p+1}\mathrm{Pr}\, Lef(\eta)\phi'(\eta) + \frac{N_t}{N_b}\theta''(\eta) = 0 \tag{13}$$

The corresponding boundary conditions (6) becomes into the Equation (14),

$$\begin{aligned} &f(0) = 0,\ f'(0) = 1,\ g(0) = 0,\ g'(0) = 0,\ \theta(0) = 1,\ \phi(0) = 1 \quad \text{at } \eta = 0 \\ &f'(\infty) \to 0,\ g'(\infty) \to 0,\ \theta(\infty) \to 0,\ \phi(\infty) \to 0 \quad \text{as } \eta \to \infty \end{aligned} \tag{14}$$

In above equations the prime symbol means the differentiation w.r.t η and non-dimensional parameters or numbers such as thermophoresis parameter N_t, materials parameters A, Brownian parameter N_b, local Reynolds number Re_x, Grashof number Gr, Lewis number Le, modified Grashof number Gm, Prandtl number Pr, radiation parameter N_r and the magnetic parameter M are defined in Equation (15),

$$\begin{aligned} &A = \frac{\mathrm{Re}_b^{\frac{2}{p+1}}}{\mathrm{Re}_x},\ \mathrm{Re}_x = \frac{U_0 x}{\upsilon},\ Gr = \frac{g\beta(T_w^* - T_\infty^*)\upsilon}{U_0^3},\ Gm = \frac{g\beta^*(C_w^* - C_\infty^*)\upsilon}{U_0^3},\ N_r = \frac{16\sigma^* T_\infty^{*3}}{3k^* k} \\ &\mathrm{Pr} = \frac{xU}{\alpha}\mathrm{Re}_b^{-\frac{2}{p+1}},\ Le = \frac{\alpha/\rho}{D_B}, M = \frac{\sigma B_0^2 \upsilon}{U_0^2 \rho}, N_b = \frac{\tau D_B (C_w^* - C_\infty^*)}{\upsilon},\ N_t = \frac{\tau D_T (T_w^* - T_\infty^*)}{\upsilon T_\infty^*} \end{aligned} \tag{15}$$

The skin friction coefficient, Nusselt number and Sherwood number are defined and denoted by

$$f''(0) = (1/2A)C_f;\quad -\theta'(0) = \mathrm{Re}_b^{-\frac{1}{p+1}} Nu_x;\quad -\phi'(0) = \mathrm{Re}_b^{-\frac{1}{p+1}} Sh_x \tag{16}$$

where $-\theta'(0)$ defines the Nusselt number, $-\phi'(0)$ represents the Sherwood number and $f''(0)$ indicates the skin friction coefficient.

Numerical simulation

In this section, the Nachtsheim-Swigert shooting iteration method along 6th order Runge-Kutta integration technique have been assumed to get the numerical solutions of the equations (10-13) with associate boundary condition in (14). Here, we try to proselytize the nonlinear ODE in the state of the system of ten first order ODE with the help of labeling variables, i.e., the reducing form of the coupled equations is in Equation (17),

$$\begin{pmatrix} F_1 \\ F_2 \\ F_3 \\ F_4 \\ F_5 \\ F_6 \\ F_7 \\ F_8 \\ F_9 \\ F_{10} \end{pmatrix} = \begin{pmatrix} f' \\ f'' \\ f''' \\ g' \\ g'' \\ g''' \\ \theta' \\ \theta'' \\ \phi' \\ \phi'' \end{pmatrix} = \begin{pmatrix} x_2 \\ x_3 \\ -\frac{1}{A}[(\frac{n(2p-1)+1}{p+1})x_1x_3 - n\{x_2\}^2 + \mathrm{Re}_x\{Grx_7 + Gmx_9 - \frac{M}{1+m^2}(x_2 + mx_5)\}] \\ x_5 \\ x_6 \\ -\frac{1}{A}[\frac{n(2p-1)+1}{p+1}x_1x_6 - nx_2x_5 + \frac{M\,\mathrm{Re}_x}{1+m^2}(mx_2 - x_5)] \\ x_8 \\ -\frac{1}{(1+N_r)}[\frac{n(2p-1)+1}{p+1}\mathrm{Pr}\,x_1x_8 + N_bx_8x_{10} + N_t\{x_8\}^2] \\ x_{10} \\ -[\frac{n(2p-1)+1}{p+1}\mathrm{Pr}\,Lex_1x_{10} + \frac{N_t}{N_b}F_8] \end{pmatrix} \quad (17)$$

along with initial conditions,

$$x_1 = f(0) = f_w = 0;\ x_2 = f'(0) = 1;\ x_3 = f''(0) = h_1;\ x_4 = g(0) = g_w = 0;\ x_5 = g'(0) = 0$$
$$x_6 = g''(0) = h_2;\ x_7 = \theta(0) = 1;\ x_8 = \theta'(0) = h_3;\ x_9 = \phi(0) = 1;\ x_{10} = \phi'(0) = h_4 \quad (18)$$

where h_1, h_2, h_3 and h_4 are the guess values of initial conditions. The iterative procedure will able to conclude whereas the error related is less than 10^{-4}.

Results and Discussion

In this segment, we try to figure out the numerical outcomes of our problem with the help of Tecplot-360 software after solving of the obtained ordinary differential. Some figures have been displayed in Figure 2 to Figure 9 to demonstrate the impact of stretching parameter *n*, magnetic parameter *M*, and Lewis number *Le* on primary velocity, secondary velocity, temperature, and concentration profiles, and a brief explanation has been provided. The values of the various parameters have been taken as $A = M = 0.5$, $m = 0.30$, $Pr = 0.71$, $N_r = Gr = Gm = 0.10$, $N_t = 0.20$, $N_b = 0.30$, $Le = 1.00$ and $Re = 1.42$.

In Figure 2, we see that the influence of stretching rate *n* on the primary velocity outlines for the Bingham fluid ($p = 0$). It is evident that the velocity outlines reduce sometimes with rising of the stretching parameter *n*. But after that the velocity outlines increasing gradually because of the increasing of the stretching parameter *n*. It is notable that the velocity profiles increase smoothly from the values of stretching parameter $n = 0.00$ to $n = 1.00$, but for the stretching parameter $n = 1.50$ and $n = 2.00$ the velocity profiles look like zigzag shaped at the interval ($\eta = 6.52000$ to $\eta = 7.24000$) for $n = 1.50$ and at the interval ($\eta = 5.16000$ to $\eta =$

5.76000) for n = 2.00. In boundary layer problem, it is investigated that the behaviors of different phenomena have been examined under the boundary layer and it is eventually noticed that in the region of boundary layer the velocity profiles look likes smooth curve. From Figure 3, it is watched that primary velocity profiles decline slightly due to the rising of the stretching rate parameter n with p = 1 and Figure 3 represents the behavior of the Newtonian fluid (p = 1). In Figure 4, it is seen that the impression of the magnetic parameter M on the primary velocity profiles and it is observed that the velocity profiles decrease due to rise the magnetic parameter M against η. Since, the magnetic parameter M directly depends on kinematic viscosity υ and inversely balanced with fluid density ϱ (From Equation 15). Hence, with the increases of the viscosity υ the velocity profiles decreases while with decreases the viscosity υ the velocity profiles increase and a quite opposite behavior is observed for the fluid density ϱ. Also, we know the magnetic field creates the Lorentz force which acts as a resistance force as a result the fluid velocity reduces with the increment of the magnetic parameter M.

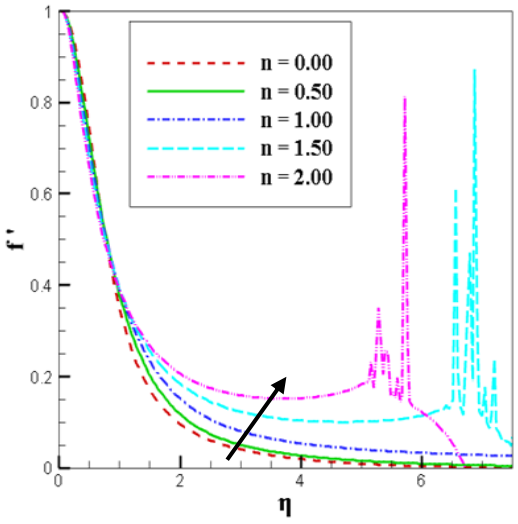

Figure 2. Impact of n on primary velocity with p = 0 (Bingham fluid).

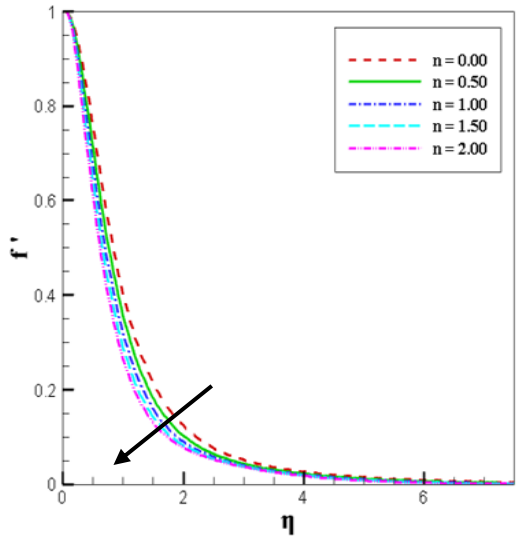

Figure 3. Impact of n on primary velocity with p = 1 (Newtonian fluid).

From Figure 5, we observed that firstly the velocity decreases because of the raising of the values of the stretching parameter n but after that it increases gradually for the Bingham fluid (p = 0). At η = 1.00 the velocity profiles decreases and the decrement rates are 0.66% from n = 0.00 to n = 0.50, 0.84% from n = 0.50 to n = 1.00, 0.63% from n = 1.00 to n = 1.50 and 0.71% from n = 1.50 to n = 2.00. Whereas at η = 3.00 the velocity profiles increases and the growth rates are 1.95% from n = 0.00 to n = 0.50, 2.45% from n = 0.50 to n = 1.00, 1.60% from n = 1.00 to n = 1.50 and 0.42% from n = 1.50 to n = 2.00 with respect to stretching parameter n. It is evident that the rate of decline at η = 1.00 is comparatively lower than the rate of growth at η = 3.00 for Bingham fluid (p = 0).

Figure 6 represents the impression of stretching parameter n on the secondary velocity profiles for Newtonian fluid (p = 1). It is noticed that the reduction of the velocity profiles with the rise of the stretching rate parameter n. The peak points of the velocity profiles for Newtonian fluid (p = 1) are 0.05452, 0.04250, 0.03524, 0.03029 and 0.02669 for the values of stretching rate parameter n = 0.00, n = 0.50, n = 1.00, n = 1.50 and n = 2.00, respectively. The decline rates are 2.40% from n = 0.00 to n = 0.50, 1.45% from n = 0.50 to n =

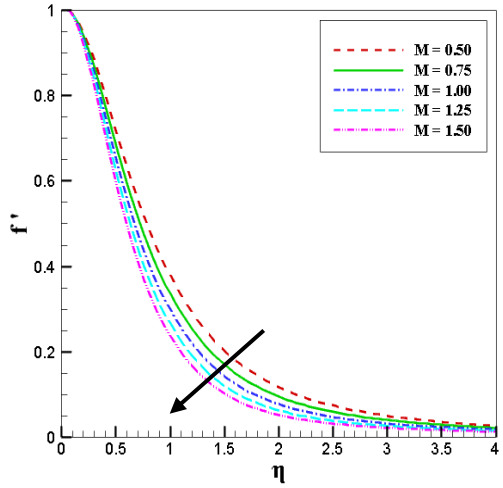

Figure 4. Primary velocity profiles due to change of M with $p = 1$.

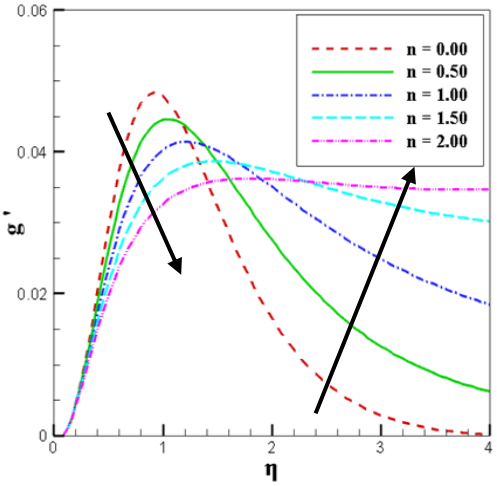

Figure 5. Impact of n on secondary velocity with $p = 0$ (Bingham fluid).

1.00, 0.99% from $n = 1.00$ to $n = 1.50$ and 0.72% from $n = 1.50$ to $n = 2.00$. It is notable that the rate of decline for Newtonian fluid ($p = 1$) is comparatively high in the interval $0 < n < 0.50$ than the other interval.

From Figure 7, it is investigated that the temperature profiles θ increases due to the increasing of the stretching parameter n in the Bingham fluid ($p = 0$) but a quite opposite behavior has been noticed from Figure 8, which is illustrated for Newtonian fluid ($p = 1$). It is also noticed from the Figure 8, the temperature profiles θ decreases and the decline rates are 1.83% ($n = 0.00$ to $n = 0.50$), 1.58% ($n = 0.50$ to $n = 1.00$), 1.36% ($n = 1.00$ to $n = 1.50$) and 1.19% ($n = 1.50$ to $n = 2.00$) at $\eta = 2.52000$ for the Newtonian fluid ($p = 1$). It is observed that the decreasing rate of Newtonian fluid ($p = 1$) is relatively lower in the interval $1.50 < n < 2.00$.

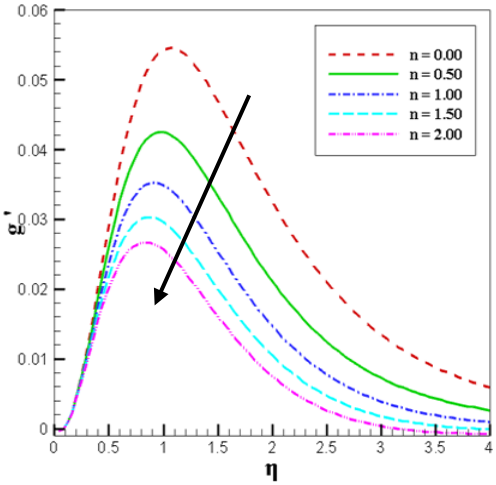

Figure 6. Impact of n on secondary velocity with $p = 1$ (Newtonian fluid).

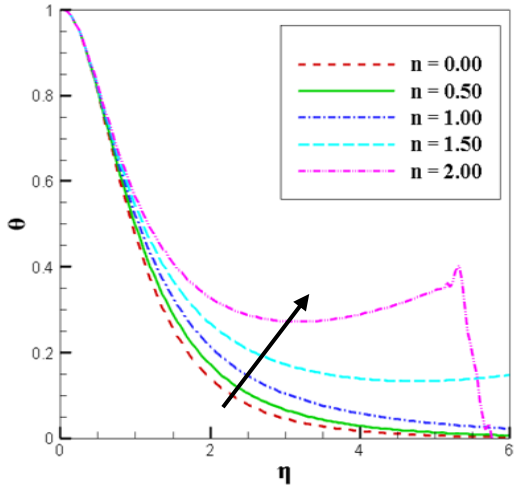

Figure 7. Impact of n on temperature profile with $p = 0$ (Bingham fluid).

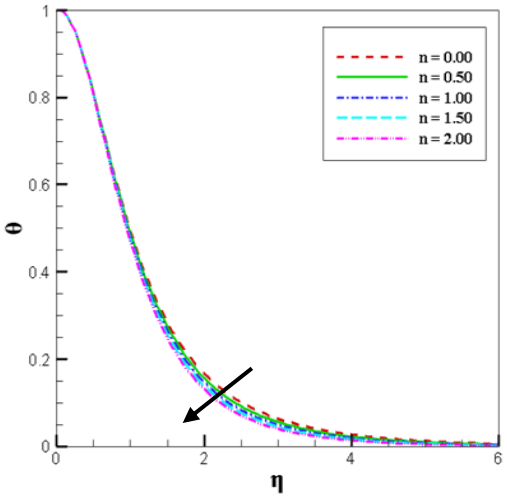

Figure 8. Impact of n on temperature profile with p = 1 (Newtonian fluid).

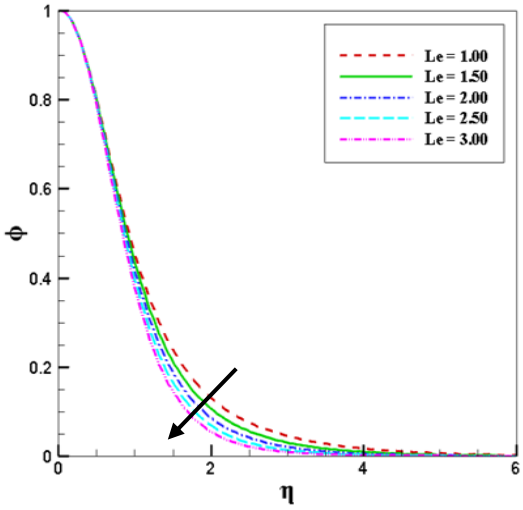

Figure 9. Concentration profiles due to change of Le with p = 1.

In Figure 9, it is seen that the concentration profiles decrease slightly with the increase of the value of the Lewis number Le. We have to know that the Lewis number Le directly proportional to the kinematic viscosity υ and opposite proportional to the Brownian motion D_B, so with the rise of kinematic viscosity υ or decline the Brownian motion D_B the concentration profiles slightly reduces and vice versa.

The impacts of stretching rate on skin friction have been seen in Figure 10 for Bingham fluid (p = 0) and Newtonian fluid (p = 1). It is observed that the skin friction grows up because of the improve of the magnitude of stretching rate n.

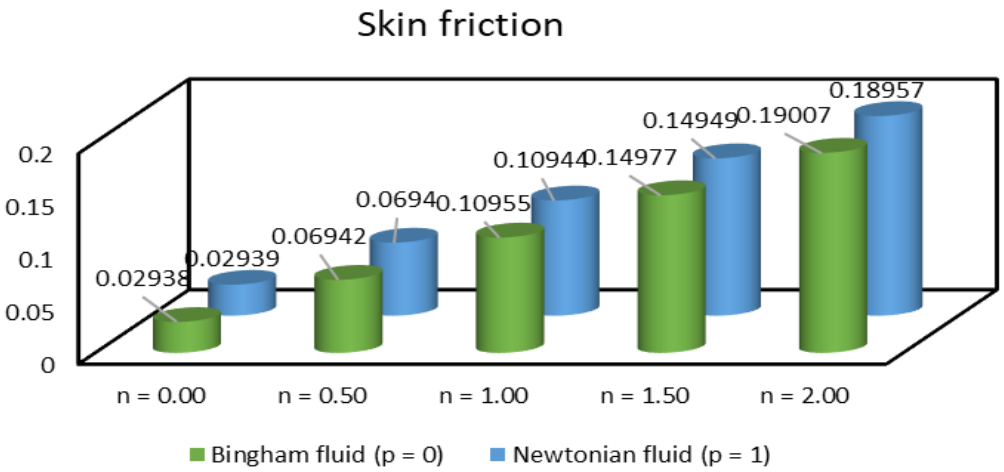

Figure 10. Influence of Stretching rate n on skin friction for different fluids.

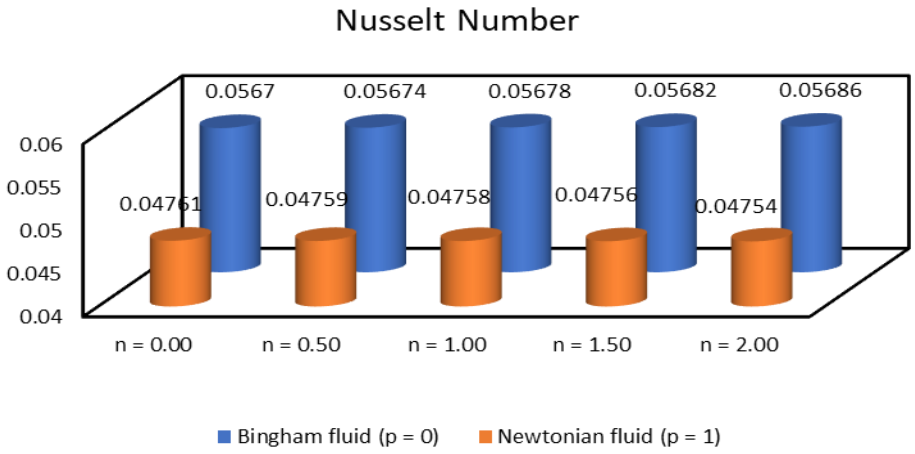

Figure 11. Influence of Stretching rate n on Nusselt number for different fluids.

The behavior of Nusselt number with the influence of stretching rate n have been illustrated in Figure 11. As the rise of stretching rate n the Nusselt number is improved for Bingham fluid ($p = 0$) but for Newtonian fluid ($p = 1$), it shows an opposite behavior though the impacts of stretching rate is very few on both fluids. In figure 11, by comparing between Newtonian fluid and Bingham fluid, it can be said that the value of Nusselt number of Bingham fluid is relatively greater than the Newtonian fluid.

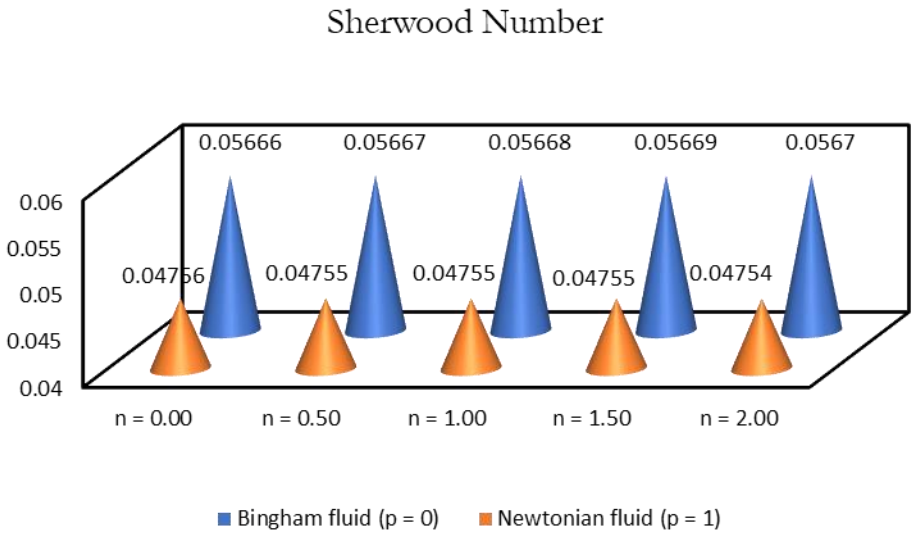

Figure 12. Influence of Stretching rate n on Sherwood number for different fluids.

In Figure 12, it can be noticed that the nature of the Sherwood number as the dominance of rate of stretching sheet n for both fluids namely Bingham fluid ($p = 0$) and Newtonian fluid ($p = 1$). The values of the Sherwood number for Bingham fluid ($p = 0$) are higher than the values of the Newtonian fluid ($p = 1$). It is

also notable that the impacts of stretching rate n is very low for both cases and opposite behavior is notable for two fluids. For Bingham fluid ($p = 0$), the Sherwood number increases as the result of the increasing the value of the stretching rate, while for Newtonian fluid ($p = 1$) its decreases.

Table 1. Tabular representation with impact of n on skin friction, Nusselt number and Sherwood number

N	Stretching rate	0.00	0.50	1.00	1.50	2.00
$p = 0$	Skin friction	0.02938	0.06942	0.10955	0.14977	0.19007
	Nusselt number	0.05670	0.05674	0.05678	0.05682	0.05686
	Sherwood number	0.05666	0.05667	0.05668	0.05669	0.05670
$p = 1$	Skin friction	0.02939	0.06940	0.10944	0.14949	0.18957
	Nusselt number	0.04761	0.04759	0.04758	0.04756	0.04754
	Sherwood number	0.04756	0.04755	0.04755	0.04755	0.04754

Table 2. Tabular representation with impact of different parameters on Skin friction

A	M	m	Gr	Re_x	Skin friction
0.50	0.50	0.30	0.10	1.42	0.06942
1.00	-	-	-	-	0.06942
1.50	-	-	-	-	0.06943
-	0.50	-	-	-	0.06942
-	0.75	-	-	-	0.09550
-	1.00	-	-	-	0.12159
-	1.25	-	-	-	0.14768
-	1.50	-	-	-	0.17379
-	-	0.30	-	-	0.06942
-	-	0.60	-	-	0.05907
-	-	0.90	-	-	0.04868
-	-	1.20	-	-	0.04057
-	-	1.50	-	-	0.03477
-	-	-	0.10	-	0.06942
-	-	-	0.30	-	0.04669
-	-	-	0.50	-	0.02397
-	-	-	0.70	-	0.00124
-	-	-	0.90	-	-0.02149
-	-	-	-	1.42	0.06942
-	-	-	-	1.52	0.07149
-	-	-	-	1.62	0.07357
-	-	-	-	1.72	0.07564
-	-	-	-	1.82	0.07771

Table 3. Tabular representation with impact of different parameter on Nusselt number and Sherwood number.

Nr	*Pr*	*Nb*	*Le*	*Re*	Nusselt number	Sherwood number
0.10	0.22	0.30	1.00	1.42	0.05674	0.05667
0.20	-	-	-	-	0.05673	0.05667
0.30	-	-	-	-	0.05673	0.05667
0.40	-	-	-	-	0.05673	0.05667
0.50	-	-	-	-	0.05673	0.05667
-	0.22	-	-	-	0.05672	0.05670
-	0.63	-	-	-	0.05673	0.05668
-	0.71	-	-	-	0.05674	0.05667
-	1.00	-	-	-	0.05674	0.05665
-	1.38	-	-	-	0.05675	0.05663
-	-	0.30	-	-	0.05674	0.05667
-	-	0.50	-	-	0.05676	0.05667
-	-	0.70	-	-	0.05679	0.05666
-	-	0.90	-	-	0.05681	0.05666
-	-	1.00	-	-	0.05682	0.05666
-	-	-	1.00	-	0.05674	0.05667
-	-	-	1.50	-	0.05674	0.05665
-	-	-	2.00	-	0.05674	0.05663
-	-	-	2.50	-	0.05674	0.05661
-	-	-	3.00	-	0.05674	0.05660
-	-	-	-	1.42	0.05674	0.05667
-	-	-	-	1.52	0.06073	0.06066
-	-	-	-	1.62	0.06473	0.06465
-	-	-	-	1.72	0.06872	0.06865
-	-	-	-	1.82	0.07272	0.07264

Table 4. Validation of this current work by comparing with previous published work

Increased Parameters	Previous results given by							Present results			
	Iva et al. (2018)				Mahmood et al. (2017)						
	U	*W*	*T*	*C*	*U*	*T*	*C*	*U*	*W*	*T*	*C*
M	*D*							*D*			
m	*I*	*I*						*I*	*I*		
Nr								*I*	*I*		
Pr			*D*			*D*				*D*	
Le							*D*				*D*
n (*p*=0)						*I*	*I*			*I*	*I*
n (*p*=1)						*D*	*D*			*D*	*D*
n (*p*=2)						*D*	*D*			*D*	*D*

**D* for Decrease, **I* for Increase.

Conclusion

The prime outcomes of our research work have been expressed as follows,

- The primary velocity profiles improve with the rise of the rate of stretching parameter n for Bingham fluid ($p = 0$), while the primary velocity profiles decrease with an improves of the rate of stretching parameter n for the Newtonian fluid ($p = 1$) and also for increasing the amount of the magnetic parameter M.
- An enhancement of the stretching rate n the secondary profiles decrease for Newtonian fluid ($p = 1$) but for Bingham fluid ($p = 0$) firstly it decreases then increases with the rise of the stretching rate n.
- With the increase of the stretching rate n, the temperature profiles θ, Sherwood number and Nusselt number have been increased for the Bingham fluid ($p = 0$), while for the Newtonian fluid ($p = 1$), the temperature profiles θ, Nusselt number and Sherwood number have been decreased. But skin friction increases with the increase of the stretching rate n for both fluids.
- An increase of the Lewis number Le concentration profiles ϕ decreases.

References

Akaje, T. W., & Olajuwon, B. I. (2021). Impacts of nonlinear thermal radiation on a stagnation point of an aligned MHD Casson nanofluid flow with Thompson and Troian slip boundary condition. *Journal of Advanced Research in Experimental Fluid Mechanics and Heat Transfer, 6*(1), 1-15.

Berrehal, H., Sowmya, G., & Makinde, O. D. (2021). Shape effect of nanoparticles on MHD nanofluid flow over a stretching sheet in the presence of heat source/sink with entropy generation. *International Journal of Numerical Methods for Heat & Fluid Flow* © Emerald Publishing Limited 0961-5539.

Bilal, S., Shah, I. A., Akgiil, A., Nisar, K. S., Khan, I., Khashan, M. M., & Yahia, I. S. (2021). Finite difference simulations for magnetically effected swirling flow of Newtonian liquid induced by porous disk with inclusion of thermophoretic particles diffusion. *Alexandria Engineering Journal, 61*, 4341–4358.

Devi, R., Poply, V., & Manimala (2021). Effect of aligned magnetic field and inclined outer velocity in Casson fluid flow over a stretching sheet with heat source. *Journal of Thermal Engineering*, Yildiz Technical University Press, Istanbul, Turkey, *7*(4), 823-844.

Haider, S. M. A., Ali, B., Wang, Q., & Zhao, C. (2021). Stefan blowing impacts on unsteady MHD flow of nanofluid over a stretching sheet with electric field, radiation and activation energy. *Coatings*, 11, 1048.

Iva, L. M., Hasan, M. S., Paul, S. K., & Mondal, R. N. (2018). MHD free convection heat and mass transfer flow over a vertical porous plate in a rotating system with hall current, heat source and suction. *International Journal of Advances Applied Mathematics and Mechanics,* 6(1), 49-64.

Khan, M. N., Ali, R., Ahmad, H., Abbas, N., Mousa, A. A. A., & Galal, A. M. (2021). Thermal and chemically reactive features of Casson nanofluid flow with thermophoresis and Brownian effect over an exponentially stretching surface. *J Process Mechanical Engineering,* 1–16.

Mahmood, T., Iqbal, Z., Ahmed, J., Shazad, A., & Khan, M. (2017). Combined effect of magnetohydrodynamics and radiation on nano Sisko fluid towards a nonlinear stretching sheet, *Results in physics*, 7, 2458-2469.

Makkar, V., & Poply, V. (2021). Impact of outer velocity on flow, heat and mass transfer of Casson nanofluid over a non-linear stretching sheet. *Journal of Thermal Engineering, 7*(6), 1353–1365.

Makkar, V., Poply, V., Goyal, R., & Sharma, N. (2021). Numerical investigation of MHD Casson nanofluid flow towards a non-linear stretching sheet in presence of double-diffusive effects along with viscous and ohmic dissipation. *Journal of Thermal Engineering*, Yildiz Technical University Press, Istanbul, Turkey, *7*(2), 1-17.

Muntazir, R. MA., Mushtaq, M., Shahzadi, S., & Jabeen, K. (2021). MHD nanofluid flow around a permeable stretching sheet with thermal radiation and viscous dissipation. *J Mechanical Engineering Science*, *0*(0) 1–16.

Ragupathi, P., Saranya, S., Mittal, H. V. R., & Al-Mdallal, Q. M. (2021). Computational study on three-dimensional convective Casson nanofluid flow past a stretching sheet with Arrhenius activation energy and exponential heat source effects. *Hindawi Complexity* Volume 2021, Article ID 5058751, 16.

Ramzan, M., Dawar, A., Saeed, A., Kumam, P., Watthayu, W., & Kumam, W. (2021). Heat transfer analysis of the mixed convective flow of magnetohydrodynamic hybrid nanofluid past a stretching sheet with velocity and thermal slip conditions. *PLoS ONE 16*(12): e0260854.

Raza, J., Dero, S., Lund, L. A., & Omar, Z. (2021). Duality and stability of MHD Darcy-Forchheimer porous medium flow of rotating nanofluid on a linear shrinking/stretching sheet: Buongiorno model. *International Journal of Numerical Methods for Heat & Fluid Flow* © Emerald Publishing Limited, 0961-5539.

Reddy, S. J., Valsamy, P., & Reddy, D. S. (2021). Radiation and heat source/sink effects on MHD Casson fluid flow over a stretching sheet with slip conditions. *Journal of Mathematical and Computational Science*, *11*(5), 6541-6556.

Sahoo, A., & Nandkeolyar, R. (2021). Entropy generation and dissipative heat transfer analysis of mixed convective hydromagnetic flow of a Casson nanofluid with thermal radiation and Hall current. *Scientific Reports*| (2021) 11:3926.

Shankaralingappa, B. M., Madhukesh, J. K., Sarris, I. E., Gireesha, B. J., & Prasannakumara, B. C. (2021). Influence of Thermophoretic Particle Deposition on the 3D Flow of Sodium Alginate-Based Casson Nanofluid over a Stretching Sheet. *Micromachines*, 12, 1474.

Thirupathi, G., Govardhan, K., & Narender, G. (2021). Radiative magnetohydrodynamics Casson nanofluid flow and heat and mass transfer past on nonlinear stretching surface. *Journal of Advanced Research in Numerical Heat Transfer*, *6*(1), 1–21.